Bull. ERS, No. 17 (1984)

LOCAL BUCKLING OF CYLINDRICAL TANKS UNDER THE HORIZONTAL LOAD

by

Yasuhiko HANGAI[I)] and Hyun Sik CHOI[I)]

INTRODUCTION

The buckling problem of cantilevered cylindrical shells is of practical importance in the design of liquid-storage tanks, containment vessels, etc. Stress distributions obtained by the linear analysis show very complicated combination of axial compression, bending and shear, and in addition are strongly influenced by the factors such as a height-to-radius ratio and a thickness-to-radius ratio. Since these stress distributions govern mainly the prebuckling state of stress, the buckling behaviour of cantilevered cylindrical shells subjected to the horizontal load, even under the assumption that the load is static, is more complicated than, for example, one of the uniformly compressed cylindrical shell. The first paper presenting a theoretical treatment to this problem is apparently due to Lundquist [1], who considered thin-walled cylinders in combined transverse shear and bending. As far as the authors are aware, there is a small number of papers published in the open literature on the theoretical analyses of cylindrical shells subjected to the transverse edge loads [2,3,4].

A cantilevered cylindrical shell subjected to a transverse shearing load at its tip has the possibility that two types of buckling such as the shear buckling and the local buckling, which appears at the lower part of the shell, may occur, as shown in Fig.1. Almost all papers [1,2,4] considered that the local buckling occurs at the support where the axial stresses are a maximum. However, the experimental results [5] show that the local buckling appears in the lower part apart from the support. This fact leads to a consideration that ovalisation by the Brazier effect makes the larger local radius of curvature than the radius of the circular cylindrical shell, and then the compressive stress level required for local buckling decreases in the part where ovalisation occurs.

On the basis of the above perspective, the paper presents an analytical method for the local buckling in consideration of ovalisation of the circular cross-section.

OVALISATION AND LOAD-DISPLACEMENT RELATION

Fig.2 shows notations for a cantilevered cylindrical shell of circular cross section with ends clamped to rigid bulkheads. Then, when the horizontal load applies to the tip of the cylindrical shell with the horizontal displacement d, the tensile and compressive longitudinal stresses on opposite sides of the neutral plane flatten the cross-section into an oval shape, as shown in the right of Fig.1. Let us assume [7] that the cross section deforms according to

$$w(\zeta,x) = a\zeta \cos 2\theta \sin \frac{\pi}{L} x \qquad (1)$$

I) Institute of Industrial Science, University of Tokyo

where w is the radial component of displacement, a and L are the radius and the length of the cylindrical shell, respectively, x is the axial coordinate whose origin is at the tip and θ is the angular coordinate. The parameter ζ is a dimensionless measure of ovalisation. In equation (1), it is assumed that rigid bulkheads preserve the original circular shape at the two ends.

The purpose of this section is to obtain two relations among the horizontal load P , the displacement d at the tip and the measure ζ of ovalisation. For this purpose, the theorem of minimum total potential energy is used.

First, let us derive the strain energy function of ovalization by using equation (1). The strain-displacement relations of a cylindrical shell are given by

$$\varepsilon_\theta = \frac{1}{a}\left(\frac{\partial u}{\partial \theta} + w\right) \tag{2}$$

$$\kappa_\theta = \frac{1}{a^2}\left(\frac{\partial u}{\partial \theta} - \frac{\partial^2 w}{\partial \theta^2}\right), \qquad \kappa_x = -\frac{\partial^2 w}{\partial x^2} \tag{3}$$

where u is the circumferential component of displacement, ε_θ is the circumferential strain, κ_θ and κ_x are the changes of curvature in the circumferential direction and in the axial direction, respectively (Fig.3). If the inextensional deformation of $\varepsilon_\theta = 0$ is assumed, we get from equation (2)

$$u(\zeta, x) = -\frac{a\zeta}{2} \sin 2\theta \sin \frac{\pi}{L} x \tag{4}$$

Introduction of equations (1) and (4) into equation (3) gives us the changes of curvature, by which the strain energy of ovalisation is obtained as

$$\begin{aligned} U_{oval} &= \frac{1}{2}\int_0^L \int_0^{2\pi} D(\kappa_x^2 + \kappa_\theta^2 + 2\,\kappa_x\,\kappa_\theta)\, a\, d\theta\, dx \\ &= \frac{\pi a D L}{4}\left[a^2\left(\frac{\pi}{L}\right)^4 + \frac{9}{a^2} + \nu\,\frac{6\pi^2}{L^2}\right]\zeta^2 \end{aligned} \tag{5}$$

where D is the bending rigidity, E and ν are Young's modulus and Poisson's ratio, respectively.

Next, let us derive the strain energy of the horizontal deformation z(x), which includes both the bending and the shear deformation. The second moment of inertia I_o for the cirlular cross-section in the original configuration is changed into

$$I(\zeta, x) = I_o\left(1 - \frac{3}{2}\zeta \sin \frac{\pi}{L} x\right) \tag{6}$$

by the oval cross-section in the deformed configuration. In equation (6), the higher order term of ζ has been neglected.

The strain energy expression by use of the bending moment M and the shearing force Q is

$$U_{beam} = \int_0^L \frac{M^2}{2EI}\,dx + \int_0^L \frac{\kappa Q^2}{2GA}\,dx \tag{7}$$

in which $G=E/2(1+\nu)$ and κ is the factor given by

$$\kappa = \int_0^{2\pi} \frac{4}{A}\left(1 + \frac{3}{2}\zeta \sin\frac{\pi}{L}x\right)^2 \sin^2\theta \; a\; t\; d\theta \tag{8}$$

If $z(x)$ is assumed to be the deformation configulation of a cantilever beam including the effect of the shear deformation, $z(x)$ is expressed by using the unknown displacement d at the tip as

$$z(x) = \frac{d}{2f}\left[\left(\frac{x}{L}\right)^3 - 3\left(\frac{x}{L}\right) + 2 + \frac{12(1+\nu)(L-x)I}{\pi\; a\; t\; L}\right] \tag{9}$$

where $$f = 1 + 6(1+\nu)\left(\frac{a}{L}\right)^2$$

The bending moment M and the shearing force Q are expressed as follows by means of $I(\zeta,x)$ and $z(x)$ in equations (6) and (9).

$$M(\zeta,x) = -EI(\zeta,x)\,\frac{d^2z(x)}{dx^2} \tag{10}$$

$$Q(\zeta,x) = \frac{d}{dx}\left[EI(\zeta,x)\,\frac{d^2z(x)}{dx^2}\right] \tag{11}$$

Introduction of equations (8), (10) and (11) into equation (7) and neglection of higher order terms of ζ lead to the strain energy U_{beam} of the horizontal deformation, namely,

$$U_{beam} = \frac{9d^2EI_o}{2\,f}\left[\frac{L^3}{3} - \frac{3}{2}\,\zeta\,\frac{\pi^2-4}{\pi^3}\,L^3\right] + \frac{9d^2\,(1+\nu)\,EI_o{}^2}{\pi at\; f^2\; L^6}\left[L + 6\zeta\,\frac{Lg}{\pi}\right] \tag{12}$$

where $$g = 1 - 4\,(1+\nu)\left(\frac{\pi a}{L}\right)^2$$

Hence the total potential energy function of ζ and d can be derived by using equations (7) and (12) as

$$U(\zeta, d) = U_{oval} + U_{beam} - P\,d \tag{13}$$

If we make partial derivatives of $U(\zeta,d)$ with respect to ζ and d, respectively, zero, we can obtain two relations among ζ, d and P.

In order to make these relations dimensionless, let us introduce the following dimensionless parameters. The classical elastic buckling stress of a uniformly compressed cylindrical shell is

$$\sigma_{c\ell} = \frac{1}{\sqrt{3(1-\nu^2)}}\,\frac{Et}{a} \tag{14}$$

In the case where the maximum axial stress at the support is the same as equation (14), the horizontal load P becomes

$$P_{c\ell} = \frac{Ea\,t^2\,\pi}{L\sqrt{3(1-\nu^2)}} \tag{15}$$

If we introduce the dimensionless parameters:

$$\bar{P} = \frac{P}{P_{c\ell}}\ ,\quad \bar{d} = \frac{d}{L}\ ,\quad \alpha = \frac{L}{a}\ ,\quad \beta = \frac{t}{a}\ ,\quad \bar{x} = \frac{x}{L} \tag{16}$$

two relations obtained by equation (13) take the form

$$\zeta = \frac{162\,(1-\nu^2)}{\pi^3\beta^2\,f^2(\pi^4/\alpha^2+9\alpha^2+6\nu\pi^2)}\left[(\pi^2-4) - 8(1+\nu)\left(\frac{\pi}{\alpha}\right)^2 g\right]\bar{d}^2 \tag{17}$$

$$\bar{P} = \frac{9\sqrt{3(1-\nu^2)}}{\alpha\beta\,f^2}\left[\frac{1}{3} + \frac{2(1+\nu)}{\alpha^2} - \left\{\frac{3}{2}\,\frac{\pi^2-4}{\pi^3} - \frac{12(1+\nu)}{\pi\alpha^2}g\right\}\zeta\right]\bar{d} \tag{18}$$

Equations (17) and (18) give two relations between ζ and $\bar{d}$ as well as between $\bar{P}$ and $\bar{d}$.

LOCAL BUCKLING

Hutchinson [6] (cf. Calladine [7]) presented a criterion of local buckling a modified form of equation (14):

$$\sigma_{cr} = \frac{1}{\sqrt{3(1-\nu^2)}}\,\frac{Et}{\rho} \tag{19}$$

where ρ is the radius of curvature of the oval cross-section at the location $\theta=3\pi/2$. This criterion is used in the paper. Since the original curvature of the cross-section is $1/a$, and the change of curvature at $\theta=3\pi/2$ is $-3\zeta(\sin\pi x/L)/a$, by $\kappa\theta$ in equation (3), then

$$\rho = \frac{a}{1-3\zeta \sin\frac{\pi}{L}x} \tag{20}$$

Substituting equation (20) into equation (19) and normalising σ_{cr} with respect to the classical buckling stress $\sigma_{c\ell}$, we obtain

$$\bar{\sigma}_{cr} = \frac{\sigma_{cr}}{\sigma_{c\ell}} = 1 - 3\zeta \sin\pi\bar{x} \tag{21}$$

Now, the maximum dimensionless axial stress at the location $\theta=3\pi/2$ takes the form

$$\bar{\sigma}_{max} = \frac{\sigma_{max}}{\sigma_{c\ell}} = \bar{P}\,\bar{x}\,\frac{1-\zeta \sin\pi\bar{x}}{1-\frac{3}{2}\zeta \sin\pi\bar{x}} \tag{22}$$

Local buckling occurs under the condition of $\bar{\sigma}_{cr}=\bar{\sigma}_{max}$, which corresponds to the intersection of the two curves, with the minimum value of $\bar{d}$. The buckling load $\bar{P}$ and the location $\bar{\ell}=1-\bar{x}$ of buckling mode for local buckling can be easily determined by this condition.

NUMERICAL EXAMPLES

Steel cylindrical shells with the length-radius ratio from 5 to 10 as well as with the thickness-radius ratio from 100 to 1000 are numerically analyzed ($E=2.1\times10^6$ kg/cm^2, $\nu=0.3$).

Fig.4 shows a dimensionless plot of the horizontal load ($\bar{P}$) and the flattening of cross-section (ζ) against the displacement ($\bar{d}$) in the case of $\alpha=5$ and $\beta=1/100$. This figure indicates that a cylindrical shell ovalises progressively under the action of a horizontal load and this ovalisation results in the decrease of the stiffness in the load-displacement relation because of the decrease of the second moment of inertia.

Fig.5 shows families of two curves of $\bar{\sigma}_{cr}$ and $\bar{\sigma}_{max}$ against the displacement ($\bar{d}$) with variable of $\bar{x}$ in the case of $\alpha=5$ and $\beta=1/100$. The bold curve BC is made by connecting intersection points of curves of $\bar{\sigma}_{cr}$ and $\bar{\sigma}_{max}$ for each value of $\bar{x}$. Local buckling occurs at the point A where the dispalcement ($\bar{d}$) reaches this intersection curve firstly. Point A in Fig.4 corresponds to this displacement on the load-displacement relation, by which we can estimate the local buckling load.

Table 1 shows the local buckling stresses at the location of the appearance of local buckling mode. The values in parentheses indicate the maximum axial stresses at the support when the local buckling occurs, and $\sigma_{c\ell}$ shows the classical buckling stresses given in equation (14). If these maximum axial stresses are larger than the yielding stress (e.g. $\sigma_y=$

2400kg/cm^2), the part of shells is in the plastic range. The values in the upper side separated by the bold line are beyond the yielding stress. For the cylindrical shells in this side, it is necessary to do the elastic-plastic buckling analysis.

Fig.6 shows the relations between $\bar{\sigma}_{cr}$ and $1/\beta$ and Fig.7 represents the relations between $\bar{\sigma}_{cr}$ and α. Dimensionless critical stresses are influenced by the values of α, but are almost constant with the change of β. Figs.8 and 9 give plots of local buckling loads against $1/\beta$ and α, respectively. These two figures are similar to Figs.6 and 7, respectively.

Figs.10 and 11 show the dimensionless measure (ζ) of the ovalisation of the cross-section at the middle of x=L/2 with variables of β and α. It is understood from Fig.10 that ζ is about from 0.12 to 0.18, according to the value of α. Figs.12 and 13 denote the dimensionless displacement ($\bar{d}$) against $1/\beta$ and α, respectively, and Figs.14 and 15 shows the dimensionless location where the local buckling appears. In the case of numerical examples adopted, $\bar{\ell}$ takes about 0.2 to 0.4. Finally, the comparison of results by numerical analyses and experiment is shown in Fig.16.

CONCLUSION

An analytical method for the local buckling is presented for cantilevered cylindrical shells subjected to a transverse load at its tip by considering the effect of ovalisation due to deformation. In the theoretical development, many assumptions such as (a) ovalisation mode (equation (1)), (b) inextensional deformation of ovalisation (ε_θ=0) and (c) deflection configuration (equation (9)) are used. However, it is made clear in the paper that the ovalisation influences strongly upon the local buckling behaviour, and also, a procedure for the theoretical analysis considering the effect of ovalisation is shown.

REFERENCES

1) Lindquist, E.E., "Strength Tests of Thin-Walled Duralumin Cylinders in Combined Transverse Shear and Bending," NACA Technical Note, No.523, 1935.

2) Schroder, P., "The Buckling Behaviour of Transverse Loaded Circular Cylinders," Technical Translation, ESRO TT-105, 1974.

3) Fisher, D.F.and Rammerstorfer, F.G., "The Stability of the Liquid-Filled Cylindrical Shells under Dynamic Loading," Buckling of Shells, Proceedings of a State-of-the-Art Colloquium, Springer, 1982, pp.569-597.

4) Galletly, G.D. and Blachut, J. "Buckling of a Cantilevered Cylindrical Shell subjected to a Transverse Shearing Force at its Tip," Third International Colloquium on Stability of Metal Structures, Paris, November 16-17, 1983.

5) Yoneda, M., Ohmori, H. and Hangai, Y., "Buckling Failure of Cantilever Type Cylindrical Shells under the Horizontal Load," Bulletin of Earthquake Resistant Structure Research Center, Institute of Industrial Science, University of Tokyo, No.15, 1982, pp.13-21.

6) Hutchinson, J.W., "Buckling and Initial Postbuckling Behaviour of Oval Cylindrical Shells under Axial Compression," Journal of Applied Mechanics, Vol.35, 1968, pp.66-72.

7) Calladine, C.R., "Theory of Shell Structures," Cambridge University Press, 1983, pp.595-625.

8) Uchiyama, K., Yamada, D. and Shiobara, K., "Buckling of Cylindrical Shells subjected to Horizontal Load," Proceedings of the Annual Convention of Architectural Institute of Japan, 1980, pp.1145-1146 (in Japanese).

9) Niwa, A. and Clough, R. W., "Buckling of Cylindrical Liquid-Storage Tanks under Earthquake Loading," Earthquake Engineering and Structural Dynamics, Vol.10, 1982, pp.107-122.

10) Shih, C. F. and Babcock, C. D., "Buckling of Cylindrical Tank under Earthquake Excitation," ASCE, Proceedings of Third Engineering Mechanics Conference, 1979, pp.81-84.

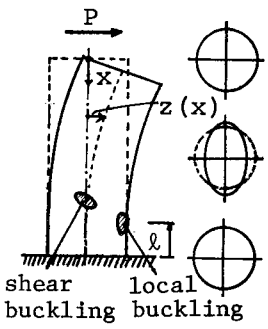

Fig.1: Deflection and Oval Deformation

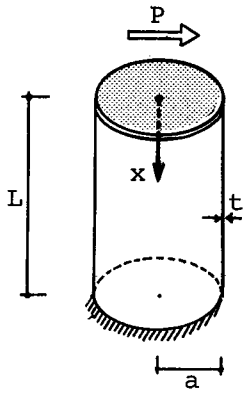

Fig.2: Cantilevered Cylindrical Shell

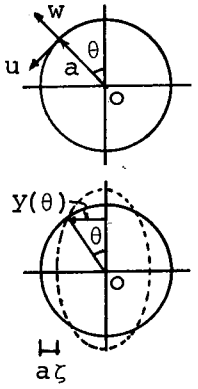

Fig.3: Displacement Components and Oval Deformation

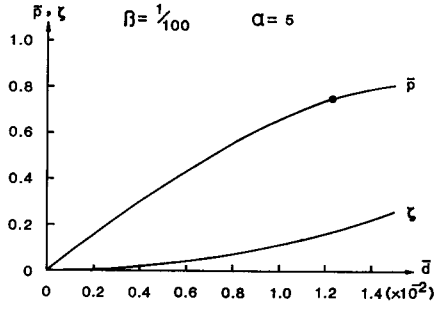

Fig.4: Horizontal Load and Flattening of Cross-Section Plotted against Displacement

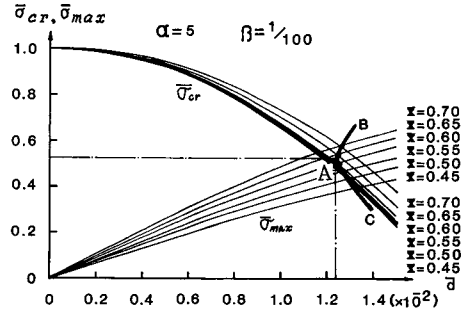

Fig.5: Relations between $\bar{\sigma}_{cr}$, $\bar{\sigma}_{max}$ and $\bar{d}$ (in the case of β=1/100 and α=5)

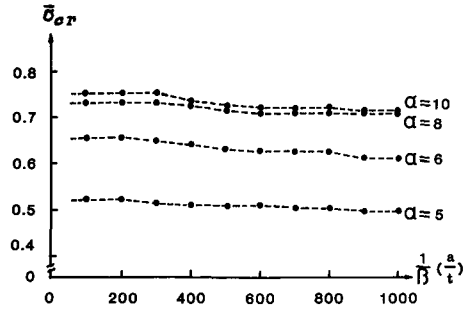

Fig.6: Relation between $\bar{\sigma}_{cr}$ and $1/\beta$

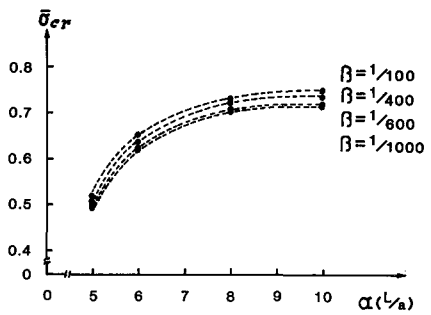

Fig.7: Relation between $\bar{\sigma}_{cr}$ and α

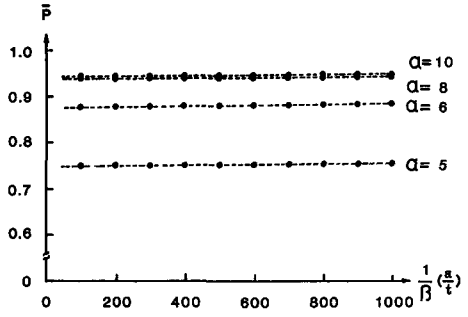

Fig.8. Dimensionless Buckling Load against $1/\beta$

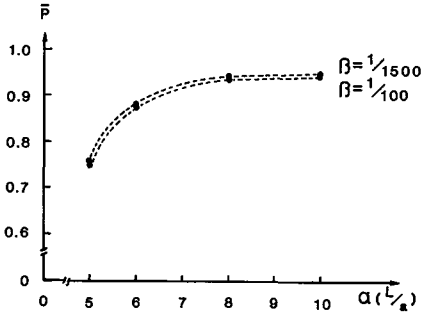

Fig.9: Dimensionless Buckling Load against α

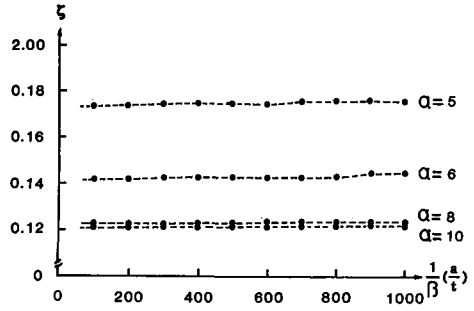

Fig.10: Relation between ζ and $1/\beta$

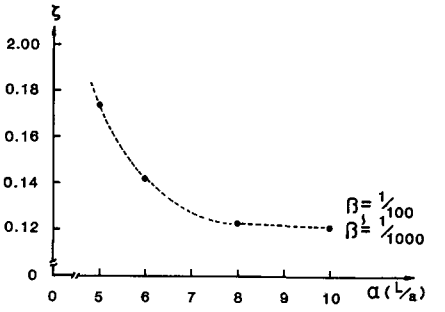

Fig.11: Relation between ζ and α

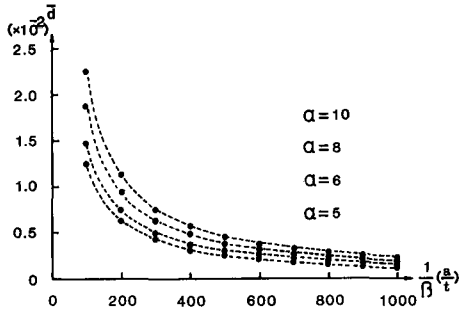

Fig.12: Dimensionless Displacement plotted against 1/β

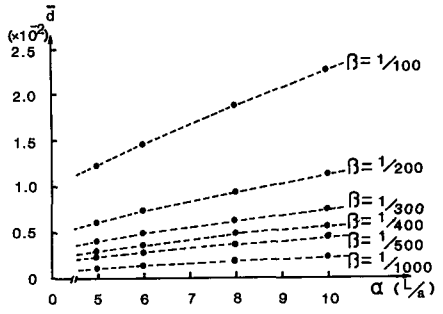

Fig.13: Dimensionless Displaceemnt plotted against α

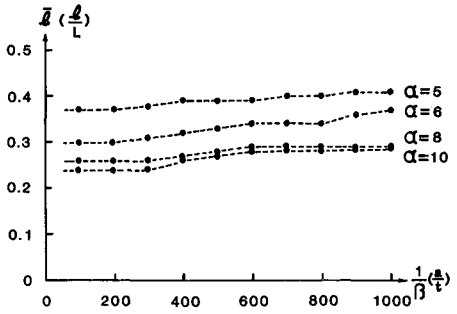

Fig.14: Location ($\bar{\ell}$) of Local Buckling against 1/β

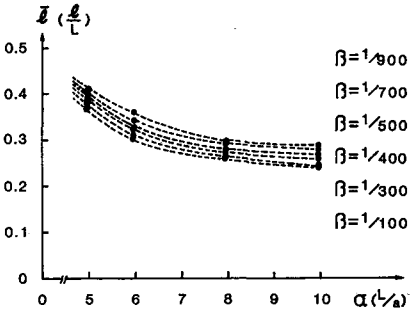

Fig.15: Location ($\bar{\ell}$) of Local Buckling against α

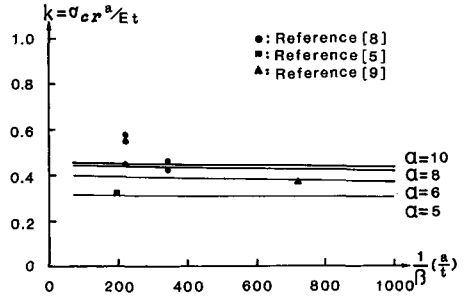

Fig.16: Comparison of Critical Stresses for Buckling

$\frac{1}{\beta}$	σ_{cl} \ α	σ_{cr} (kg/cm^2) 5	6	8	10
100	12,705	6,619 (9,516)	8,321 (11,095)	9,287 (11,955)	9,541 (11,993)
200	6,352	3,309 (4,757)	4,160 (5,564)	4,643 (5,964)	4,770 (5,996)
300	4,235	2,172 (3,176)	2,740 (3,709)	3,095 (3,976)	3,180 (3,997)
400	3,176	1,610 (2,382)	2,029 (2,785)	2,296 (2,985)	2,331 (2,998)
500	2,541	1,288 (1,095)	1,603 (2,228)	1,816 (2,391)	1,844 (2,401)
600	2,117	1,073 (1,587)	1,321 (1,856)	1,496 (1,994)	1,520 (2,002)
700	1,815	907 (1,367)	1,132 (1,591)	1,283 (1,708)	1,303 (1,715)
800	1,588	794 (1,192)	891 (1,394)	1,122 (1,496)	1,140 (1,502)
900	1,411	695 (1,061)	859 (1,241)	997 (1,329)	1,002 (1,336)
1000	1,270	626 (953)	763 (1,120)	897 (1,195)	901 (1,202)

ν=0.3 E=2,100,000Kg/Cm^2

Table 1: Critical Stresses for Local Buckling